TISSUE ENGINEERING: Part A
Volume 27, Numbers 15 and 16, 2021

DOI: 10.1089/ten.tea.2020.0218

termis
Tissue Engineering
& Regenerative Medicine
International Society

ORIGINAL ARTICLE

Combination of BMP2 and EZH2 Inhibition to Stimulate Osteogenesis in a 3D Bone Reconstruction Model

Hayman Lui, MD, PhD,[1–3] Rebekah M. Samsonraj, PhD,[2,3] Cedryck Vaquette, PhD,[4]
Janet Denbeigh, PhD,[2,3] Sanjeev Kakar, MD,[2] Simon M. Cool, PhD,[5]
Amel Dudakovic, PhD,[2,3] and Andre J. van Wijnen, PhD[2,3]

High concentrations of bone morphogenetic protein 2 (BMP2) in bone regeneration cause adverse events (e.g, heterotopic bone formation and acute inflammation). This study examines novel epigenetic strategies (i.e., EZH2 inhibition) for augmenting osteogenesis, thereby aiming to reduce the required BMP2 dose *in vivo* for bone regeneration and minimize these adverse effects. Human bone marrow-derived mesenchymal stem cells (BMSCs) were grown on three-dimensional (3D)-printed medical-grade polycaprolactone scaffolds and incubated in osteogenic media containing 50 ng/mL BMP2 and/or 5 μM GSK126 (EZH2 inhibitor) for 6 days ($n = 3$ per group and timepoint). Constructs were harvested for realtime quantitative polymerase chain reaction analysis at Day 10 and immunofluorescence (IF) microscopy at Day 21. After pretreating for 6 days and maintaining in osteogenic media for 4 days, BMSC-seeded scaffolds were also implanted in an immunocompromised subcutaneous murine model ($n = 39$; 3/group/donor and 3 control scaffolds) for histological analysis at 8 weeks. Pretreatment of BMSCs with BMP2 and BMP2/GSK126 costimulated expression of osteoblast-related genes (e.g., *IBSP*, *SP7*, *RUNX2*, and *DLX5*), as well as protein accumulation (e.g., collagen type 1/*COL1A1* and osteocalcin/*BGLAP*) based on IF staining. While *in vivo* implantation for 8 weeks did not result in bone formation, increased angiogenesis was observed in BMP2 and BMP2/GSK126 groups. This study finds that BMP2 and GSK126 costimulate osteogenic differentiation of MSCs on 3D scaffolds *in vitro* and may contribute to enhanced vascularization when implanted *in vivo* to support bone formation. Thus, epigenetic priming with EZH2 inhibitors may have translational potential in bone healing by permitting a reduction of BMP2 dosing *in vivo* to mitigate its side effects.

Keywords: regenerative medicine, tissue engineering bone formation, orthopedic surgery, BMP2, EZH2, epigenetics

Impact Statement

While autografts are still the gold standard for bone reconstruction, tissue availability and donor morbidity are significant limitations. Previous attempts to use high concentrations of bone morphogenetic protein 2 (BMP2) have been shown to cause adverse events such as excessive bone formation and acute inflammation. Overall, the utilization of EZH2 inhibitors to modulate gene expression in favor of bone healing has been demonstrated *in vitro* in a tissue engineering strategy. Our study will pave the way to developing tissue engineering strategies involving GSK126 as an adjuvant to increase the effects of BMP2 for stimulating cells of interest on a three-dimensional scaffold for bone regeneration.

[1]School of Medicine, Griffith University, Gold Coast, Queensland, Australia.
Departments of [2]Orthopedic Surgery and [3]Biochemistry and Molecular Biology, Mayo Clinic, Rochester, Minnesota, USA.
[4]School of Dentistry, The University of Queensland, Brisbane, Queensland, Australia.
[5]Glycotherapeutics Group, Institute of Medical Biology, Agency for Science, Technology and Research (A*STAR), Singapore, Singapore.

Introduction

AUTOLOGOUS BONE GRAFTS have been used extensively in the medical field to fill craniofacial and long bone defects.[1–4] While autografts are still the gold standard for bone reconstruction, tissue availability, donor morbidity, and graft resorption are significant limitations. Therefore, biomaterials of various origins have been developed to circumvent these limitations and the recent advancement in rapid prototyping technologies such as three-dimensional (3D) printing with orthoconductive scaffolds have shown the promise of customized implants and personalized medicine.

Scaffold material for bone tissue engineering includes ceramics (calcium phosphates), hydroxyapatite (HA), bioglasses, polymers (collagen, chitosan, polylactide), and hybrid materials.[5–7] Ceramics are advantageous due to their excellent bioactivity but are inherently brittle. This makes it difficult for clinical translation, as the scaffolds cannot be fixed with screws. Other scaffolds such as collagen sponges,[8,9] silk scaffolds,[10] collagen,[11] or alginate[12] hydrogels for facilitating bone morphogenetic protein 2 (BMP2) release have also been shown to demonstrate good bone formation in bone defect models.

On the contrary, polymers lack bioactivity but are ductile and have superior mechanical properties in comparison with other biomaterials. The use of medical-grade polycaprolactone (mPCL) in bone regeneration is appropriate for this study as it allows the tissue-engineered construct to withstand greater mechanical forces and offers greatest flexibility for surgical fixation. In fact, numerous studies have investigated the use of mPCL for bone regeneration.[13–15] Therefore, mPCL is the most suitable biomaterial to use for *in vitro* culture when examining the full effects of BMP2 and/or GSK126.

A bone tissue-engineered construct is traditionally manufactured by seeding cells of interest such as bone marrow stromal cells or osteoblasts and culturing them under a differentiation cocktail *in vitro* before implantation. Cellular differentiation is usually performed by directly upregulating bone-related genes and this is achieved by the addition of osteogenic compounds in the culturing media. While the biochemical composition of the differentiation media and the length of culture required to achieve sufficient cell stimulation for triggering bone formation are still debatable,[16,17] this concept underpins the manufacturing of tissue engineering products. In addition to the use of a scaffold for 3D cell culture, the addition of growth factors can be used to promote osteogenesis.

Key factors in bone regeneration include the TGF-β family signaling molecules in which BMPs are a major subset. BMPs were first discovered by Urist in the 1980s[18] and are extracellular cytokines that have endocrine, paracrine, and autocrine signaling functions. They have an essential role in maintaining bone homeostasis and embryological development. In particular, bone regeneration has been clinically triggered by the delivery of osteogenic cues such as BMP2 directly influencing cell commitment to osteogenesis through the Smad-dependent or Smad-independent pathways.[19–24]

Beyond the Smad pathway, gene expression during osteoblastogenesis is modulated by changes in the structure and topology of DNA, which is packaged by histones into nucleosomes to form chromatin.[25] This epigenetic regulation, which allows for preservation of the DNA genotype while inducing changes in cellular phenotype,[26] occurs through the modulation of key transcription factors, as well changes in DNA methylation, histone modifications, mitotically transmitted messenger RNAs (mRNAs), small-coding RNAs (mRNAs), long noncoding RNAs (lncRNAs), and mitotic bookmarking.[27–32] Gene expression of osteogenic-related markers is epigenetically controlled by enhancer of zeste homologue 2 (EZH2), the active subunit of polycomb-repressive complex 2 (PCR2), which methylates histone 3 at lysine 27 (H3K27) during bone formation.[33–38] Trimethylation of H3K27 by EZH2, which forms H3K27me3 marks gene regulatory regions, induces heterochromatin formation to inhibit gene expression. Suppression of EZH2 protein levels and activity has been shown to stimulate osteogenic differentiation *in vitro* as well as enhances bone formation and prevents estrogen depletion-induced bone loss *in vivo*.[34–36,39–45] Results from other studies have also indicated that overexpression of EZH2 results in adipogenic differentiation of MSCs.[42,46] Mechanistically, inhibition stimulates expression of key intermediates of bone stimulatory pathways (e.g., BMP2, WNT, and PTH signaling) to stimulate osteogenic differentiation.[34]

EZH2 is an attractive target for pharmacological strategies to promote new bone, because extensive safety data are available for drugs targeting this protein based on cancer-related studies. For example, abnormal EZH2 activity has been associated with lymphoma,[47] breast,[48] and prostate[49] cancer progression, because EZH2 has been functionally linked to cellular proliferation, metastasis, and DNA repair.[50] GlaxoSmithKline 126 (GSK126) is one well-characterized EZH2 inhibitor shown to inhibit lymphoma growth and is currently in clinical trials for application in treating B cell lymphoma.[51] While the cytostatic activity of EZH2 would not permit long-term systemic applications as a potential bone anabolic, short-term local applications or pretreatment of osteogenic cells with drugs that target EZH2 may be a valuable strategy to promote bone healing.

The principal goal of this study is to assess the concept of combining BMP2 with epigenetic priming by an EZH2 inhibitor (GSK126) to pretreat a 3D cell culture of human bone marrow mesenchymal stem cells (BMSCs) for promoting bone healing. Therefore, we assessed the *in vitro* efficacy of the EZH2 inhibitor GSK126, with or without a low-dose BMP2, toward the differentiation of human bone marrow-derived mesenchymal stem/stromal cells (BMSCs) grown on scaffolds. In this study, BMSCs were directly seeded onto a highly porous 3D-printed scaffold suitable for bone regeneration and preconditioned by cotreatment with BMP2 and GSK126 as optimized in previous studies in our laboratory.[34,35,44] The osteogenic commitment of the cells was examined by expression of selected genes involved in bone formation. Furthermore, the *in vivo* impact of cell preconditioning with the addition of BMP2 and/or GSK126 was assessed in a murine subcutaneous model.

Materials and Methods

3D printing

Continuous printing of PCL results in fabrication of properly connected fibers forming a construction with 0/90° between layers and a 600 μm fiber interdistance, as previously described.[52] Each layer had a thickness of 467 ± 34 μm. A 5 or 3 mm biopsy punch (Thermo Fisher Scientific, Waltham, MA) was used to create circular discs for use in the following experiments due to technical limitations in 3D printing small parts.

BMSC extraction and cell culture

The BMSCs from three different male donors aged between 20 and 30 years (1A, 2A, and 3A) were isolated using plastic adherence from the bone marrow mononuclear cells (Cat. no. 2M-125; Lonza, Basel, Switzerland) as described previously.[53] Briefly, human bone marrow mononuclear cell fractions were plated in maintenance medium comprising Dulbecco's modified Eagle's medium (DMEM) with 10% fetal calf serum (Hyclone, San Angelo, TX), 2 mM L-glutamine, 50 U/mL penicillin, and 50 U/mL streptomycin (Sigma Aldrich, St Louis, MI). Cells were allowed to adhere for 7 days and nonadherent cells in the medium were subsequently removed. Adherent cells were allowed to form colonies and expand for 3–5 weeks, following which they were harvested and replated at a density of 5000 cells per cm^2 and expanded for 4–6 passages. Cells from passage 4–6 were seeded on PCL scaffolds for use in all *in vitro* and *in vivo* scaffold-based experiments. Basal cell culture medium was a combination of α modified Eagle's medium (αMEM) with 10% fetal bovine serum and 1% penicillin/streptomycin (Gibco, Waltham, MA). Osteogenic differentiation medium included the addition of ascorbic acid (50 μg/mL), β-glycerol phosphate (10 mM), and dexamethasone (10 nM).

Cell seeding onto PCL scaffolds

Scaffold preparation and sterilization. Scaffolds were first etched by immersion in 5 M NaOH at 37°C for 30 min before being washed three times (5-min duration) with distilled water. Scaffolds were incubated in 100% ethanol at room temperature for 30 min before being sterilized under UV light for 30 min as previously described.[54–56]

Loading of dynamic bioreactor for cell seeding onto scaffolds. Cells were seeded in the scaffold using a dynamic bioreactor (Synthecon RCCS4H, Houston, TX) in a cell suspension density of 1 million cells/mL/scaffold. After 24 h in the bioreactor, the seeded scaffolds were transferred to a poly-2-hydroxyethyl methacrylate (poly-HEMA)-coated 48-well plate (to avoid cell attachment to plate surface) and further cultured with 5 μM GSK126 (Sigma Aldrich), 50 ng/mL BMP2 (R&D Systems, Minneapolis, MN), or a combination of both BMP2 and GSK126 in osteogenic medium for 6 days. The concentrations of BMP2 and GSK126 were chosen based on the results of previous studies carried out by our group.[34,35] The medium was changed every 2 days.

Five different groups were created for the study: scaffold with BMSCs cultured in basal medium (Group 1: Control), scaffold with BMSCs cultured in osteogenic medium (Group 2: Osteo), scaffold with BMSCs cultured in osteogenic medium with BMP2 (Group 3: BMP2), scaffold with BMSCs cultured in osteogenic medium with GSK126 (Group 4: GSK126), scaffold with BMSCs cultured in osteogenic medium with both BMP2 and GSK126 (Group 5: BMP2/GSK126). These groups ($n = 3$ per treatment) were replicated for each of the three donors used (1A, 2A, and 3A).

After 6 days of treatment with BMP2 and/or GSK126, cultures of seeded scaffolds were maintained on osteogenic medium for another 4 days. At 10 days, samples were harvested and utilized in a variety of assays (described below); live-dead assay, scanning electron microscopy (SEM), RNA extraction for realtime quantitative polymerase chain reaction (RTqPCR), immunofluorescence (IF), and ectopic implantation with hematoxylin and eosin (H&E) or Sirius red staining ($n = 3$ per group per donor). To evaluate the long-term influence of cell preconditioning upon bone-related protein secretion (collagen type I/*COL1A1* and osteocalcin/*BGLAP*), the constructs were subsequently cultured in osteogenic medium for 21 days and IF was utilized to visualize these proteins. Similarly, the influence of preconditioning on cell viability at Days 10 and 21 was investigated for the BMP2/GSK126 group and compared with cells cultured under osteogenic condition.

In vitro *characterization*

Assessment of the preconditioning long-term effect

Cell viability. The impact of the PCL scaffold and bioreactor environment on the BMSCs was assessed by measuring cell viability at Days 10 and 21 for the Osteo and BMP2/GSK126 groups. Seeded scaffolds ($n = 3$ per culture conditions) were stained with calcein acetoxymethyl (1:500 dilution) and ethidium homodimer-1 (1:2000 dilution) according to the manufacturer's instructions (Live/Dead Viability/cytotoxicity kit for mammalian cells; Invitrogen Molecular Probes, Waltham, MA) and incubated for 20 min before visualization using an inverted LSM 780 multiphoton laser scanning confocal microscope at excitation wavelengths of 488 and 561 nm.

Scanning electron microscopy. To characterize the constructs under osteogenic and BMP2/GSK126 preconditioning at Day 10, the cellularized scaffolds ($n = 3$) were fixed in Trumps fixative at 4°C for 1 h, washed in phosphate-buffered saline (PBS), rinsed in water, and dehydrated through a graded series of ethanol. They were then critical point dried using CO_2. These samples and control noncellularized scaffolds ($n = 3$) were then mounted on an aluminum stub and sputter-coated for 150 s with gold-palladium. Samples were imaged in a Hitachi S-4700 cold field emission scanning electron microscope at 5 kV accelerating voltage. Average strut diameter was calculated from measurements of five different images.

Assessment of the osteogenic differentiation

Quantitative realtime qPCR. The impact of cell preconditioning on osteodifferentiation was investigated using a number of the downstream genes activated in osteogenesis: integrin-binding sialoprotein (*IBSP*), osterix/SP7 transcription factor (*SP7*), runt-related transcription factor 2 (*RUNX2*), and distal-less homeobox 5 (*DLX5*). In particular, the expression of *IBSP* encodes a protein that specifically binds calcium and HA and constitutes a major component of noncollagenous proteins in bone. On the contrary, *SP7*, *Runx2*, and *DLX5* are important BMP2 responsive transcription factors essential for osteoblast differentiation.

To evaluate gene expression of these osteogenic markers at the mRNA level, total RNA was isolated from control and treatment groups (osteogenic medium with or without BMP2, GSK126, BMP2/GSK126) at Days 0 and 10 post-treatment by TRIzol-based extraction. RNA extraction was completed as per the Direct-zol RNA Isolation Miniprep Protocol. Using the SuperScript III First-Strand Synthesis System (Invitrogen), complementary DNA (cDNA) was prepared and used as a template for real-time PCR in an SYBR Green-based

reaction. Samples were run on a CFX384 RealTime qPCR System (BioRad, Hercules, CA). Previously validated primer sequences were used to amplify cDNAs for genes of interest, including *IBSP*, *SP7*, *Runx2*, and *DLX5* (Table 1). Gene expression was quantified by the $2^{-\Delta\Delta Ct}$ method and presented as relative expression units normalized to a single housekeeping gene, GAPDH.

IF microscopy. To evaluate the relative presence of bone-related proteins, the BMSC-laden PCL scaffolds that underwent osteogenic differentiation with or without BMP2 and GSK126 for 21 days were fixed in 4% paraformaldehyde (PFA) for 10 min before proceeding for immunostaining. The samples were rinsed in PBS twice and subsequently blocked with 2.5% BSA in PBS for 1 h, and incubated with primary antibodies to human collagen 1 (C2456, 1:500 dilution; Sigma) and human osteocalcin (ab13421, 1:200 dilution; Abcam) in 1% BSA overnight at 4°C with gentle shaking. After removing the primary antibodies, samples were washed three times with PBS and incubated with corresponding secondary antibodies (goat anti-rabbit IgG [Alexa Fluor 488, ab150077; Abcam] and donkey anti-rabbit [Alexa Fluor 594, ab150108; Abcam]) for 1 h at room temperature. Using established and constant settings, samples were imaged by confocal microscopy and z-stacks were collected for each sample, with ~50 slices. The number of pixels (green or red) per channel for a set area was then quantified using ImageJ normalizing by the cell number to estimate the relative amount of protein synthesized.

Alizarin red staining. To evaluate mineralization, donor BMSC-laden PCL scaffolds with or without preconditioning were treated in osteogenic conditions for 21 days and thereafter fixed in 4% PFA for 10 min and washed with PBS. This was followed by staining with 0.1% Alizarin red solution (pH 4.2) for 30 min at room temperature, followed by several gentle washes with distilled water. Scaffolds were allowed to air-dry and then scanned using an Epson Perfection V600 scanner. For semiquantification of the Alizarin red staining, 200 μL of 10% acetic acid was added to each well of the 24-well plate and incubated for 30 min with shaking. This was transferred to a 1.5 mL microcentrifuge tube and vortexed vigorously for 30 s. The pH was adjusted with ~75 μL 10% ammonium hydroxide ensuring that the pH was within the range of 4.1–4.5. Aliquots of 50 μL for each sample were transferred to an opaque-walled, transparent-bottom, 96-well plate, and the solution absorbance was read at 405 nm. The results were averaged over the donors and displayed as raw absorbance values.

In vivo *implantation*

The efficacy of the different groups toward ectopic bone formation was assessed using a subcutaneous murine model. To this end, female mice with severe combined immune deficiency (Envigo, Indianapolis, IN), between the ages of 8–10 weeks, were used for this study. All procedures were followed in accordance with Mayo Clinic's Institutional Ethics-Approved Small-Animal Protocol (IACUC#A00002695-17). The experimental groups included PCL scaffold alone (Control) and the cell-laden scaffolds in combination with BMSCs treated with osteogenic medium (Osteo), BMP2, GSK126, and a combination of BMP2/GSK126, resulting in a total of five groups per donor MSC and three implants per group. After 6 days of treatment with BMP-2 and/or GSK126, cell culture of seeded scaffolds was maintained on osteogenic medium for another 4 days. This enabled both cell differentiation and the re-establishment of the proliferative capacity before *in vivo* implantation. At 10 days, samples were harvested and ectopic implantation was performed adopting a random assignment design, with up to 2 implants per animal. In total, 39 scaffolds were implanted into 20 mice with up to two scaffolds per side.

Before implantation, the scaffolds were injected with a heparinized gelatin-hyaluronic-acid hydrogel to provide natural extracellular matrix (ECM) in the direct vicinity of the cells. Therefore, 25 μL of the heparinized gelatin/hyaluronic acid hydrogel (Sigma Aldrich) was reconstituted as per the manufacturer's instructions for reaching a 1%wt/vol hydrogel composition and carefully dispensed into the seeded scaffold. The scaffolds were incubated at 37°C, 5% CO_2 for ~20 min allowing the gel to set before implantation.

Animals were anesthetized using isoflurane. After induction of anesthesia, the hair on the dorsal site of surgery was clipped and the skin was cleaned with iodine and ethanol swabbing. Using a sterile scalpel, a 1 cm incision was made dorsally on the skin on either side of the midline. A subcutaneous pocket was created and the scaffolds were implanted (one implant per pocket) (Appendix Fig. 1A), followed by closure of the incision using sterile wound clips (Appendix Fig. 1B, C). After the surgery, the animals were placed on a heating pad to recover from anesthesia before returning them to their cages. After 2 weeks, the wound clips were removed. After 8 weeks, the animals were sacrificed and the implants harvested and transferred to 4% paraformaldehyde for fixation and histological processing.

microCT. Samples were analyzed by microCT (μCT40, SCANCO Medical AG, Brüttisellen, Switzerland) with a voltage of 45 kVp, a current of 177 μA and power of 4 W, an integration time of 200 ms, a voxel size of 20 μm, and a grayscale threshold of 220 to determine bone mineralization. Three-dimensional images were reconstructed using the microCT software.

Table 1. Forward and Reverse Gene Primers Used in Real Time Quantitative Polymerase Chain Reaction Analysis

Gene	*Forward*	*Reverse*
GAPDH	ATGTTCGTCATGGGTGTGAA	TGTGGTCATGAGTCCTTCCA
IBSP	GAACCTCGTGGGGACAATTAC	CATCATAGCCATCGTAGCCTTG
SP7	GCCATTCTGGGTTGGGTATC	GAAGCCGGAGTGCAGGTATCA
RUNX2	TGGTTACTGTCATGGCGGGTA	TCTCAGATCGTTGAACCTTGCTA
DLX5	AGCTACGCTAGCTCCCTACCACC	GGTTTGCCATTCACCATTCTCAC

Histology

H&E and Sirius red staining. To characterize the *in vivo* constructs, the samples were dehydrated and paraffin embedded using a tissue processor (Shandon™ Excelsior ES; Thermo Scientific, Waltham, MA). Five-micrometer cross-sectional slices of the constructs were sectioned and collected on polylysine-coated slides. These samples were deparaffinized with xylene before rehydration with decreasing concentrations of ethanol. Sections were stained with H&E and Sirius red and scanned with an Aperio AT2 Console (Leica Biosystems Imaging, Inc.).

Histomorphometry. Histomorphometry was conducted on the samples stained with H&E using the ImageScope suite. The number of blood vessels and the surface area occupied by early stages of mineralization, as well as the remaining hydrogel in the scaffold, were measured to quantify the performance of the different scaffold designs.

Statistics

One-way analysis of variance was used for determining statistical significance in cell viability, gene expression IF, and histomorphometry. A $p \leq 0.05$ was considered to represent statistically significant differences.

Results

Scaffold characterization

The architecture of PCL scaffolds by continuous 3D printing was evaluated by SEM analysis. The results revealed uniform mPCL struts of 467 ± 34 μm diameter at alternating 0/90° (Fig. 1A, B). As the average cell diameter of fibroblastic BMSCs is between 10 to 30 μm, this geometry provides sufficient substratum for cell attachment while permitting gas exchange and solute diffusion with the culture media.

In vitro *characterization*

Cellularized scaffolds. At both Days 10 and 21, there was a statistically significant decrease in the percentage of live cells for given culture conditions ($p < 0.05$) (Fig. 1C). The addition of BMP2 and GSK126 did not adversely affect cell viability on Day 10. Interestingly, the later time point demonstrated that preconditioning with BMP2/GSK126 resulted in a slight decrease in the cell viability when compared with osteogenically induced cells. SEM analysis of the cellularized constructs showed extensive ECM deposition within scaffold pores (Fig. 1E). Similar matrix lattices were observed in both Osteo and BMP2/GSK126 treatment groups.

Assessment of osteogenic differentiation

RTqPCR. To mitigate the effects of donor variation on gene expression, realtime qPCR data results were assessed separately for each donor-derived BMSC population. Although the gene expression differed between donors, the pattern of expression was consistent for most genes assessed in our analysis. More specifically, *IBSP* was upregulated by BMP2 and BMP2/GSK126 in the majority of donors (Fig. 2A) and reached statistical significance ($p = 0.05$) for Donor 2A when the BMP2/GSK126 was compared with the Control, Osteo, and GSK126 groups. Similarly, *SP7* was upregulated in the BMP2/GSK126 treatment with the majority of donors showing a significant difference when compared against the Control, Osteo, and GSK126 groups (Fig. 2B).

The expression of *RUNX2* was significantly upregulated by BMP2/GSK126 treatment against Control and Osteo conditions for Donor 2A and against all other conditions in Donor 3A (Fig. 2C). For most genes and donors, BMP2 and GSK126 treatment alone had a similar effect to Osteo media but still demonstrated higher levels of expression when compared with the Control. Finally, *DLX5* was upregulated in the BMP2 and BMP2/GSK126 conditions and had significantly higher expression than the control condition in Donors 2A and 3A (Fig. 2D). Conversely, GSK126 treatment yielded significantly less *DLX5* expression compared with the BMP2/GSK126 group in Donor 3A, but a similar level of expression compared with the Control and Osteo groups. Overall, this experiment demonstrated that the utilization of BMP2-GSK126 in the media consistently upregulated the expression of genes involved in osteogenesis.

Immunofluorescence. Collagen type I (*COL1A1*) and osteocalcin (*BGLAP*) are key markers of the ECM in bone (respectively, most abundant collagen and noncollagenous protein) and the presence of these proteins was detected *in vitro* after 21 days of culture (Fig. 3A–E). Semiquantification of the IF staining (Fig. 3I, J) demonstrated that across the donors, BMP2 and BMP2/GSK126 treatment resulted in the upregulation of *COL1A1* (red) and *BGLAP* (green) protein expression. In particular, the BMP2/GSK126 treatment group for Donor 1A had significantly higher levels of expression of both *COL1A1* and *BGLAP* when compared with the other groups ($p < 0.05$). This trend was similarly seen in *COL1A1* expression for Donor 3A, but there was no statistical difference between the BMP2 and BMP2/GSK126 groups. *BGLAP* expression for Donor 3A demonstrated statistically significant differences between the BMP2 group compared with the Control, Osteo, and GSK126 groups ($p < 0.05$). There was no significant difference between BMP2 and BMP2/GSK126 treatment groups.

For Donor 1A, there was a significantly lower *COL1A1* and *BGLAP* protein deposition in the GSK126 group when compared with the rest of the treatment groups ($p < 0.05$). Interestingly, while Donor 1A exhibited the most difference in protein synthesis, this trend was not seen in gene expression. Incubation of the scaffolds with no cells as well as with secondary antibodies alone did not demonstrate nonspecific staining (Fig. 3F–H).

Alizarin red staining. Semiquantification of the staining on scaffolds cultured with BMP2 and/or GSK126 for 21 days *in vitro* showed that all treatment groups (control excluded) had an effect in upregulating calcium deposition (Fig. 4A). The control groups displayed positive staining, which can be attributed to nonspecific Alizarin red binding. When the results were averaged for the three donors (Fig. 4B), the BMP2 treatment group had the greatest amount of *in vitro* mineralization although it did not reach statistical significance when compared with the other treatment groups. It can also be seen that GSK126 has an effect on bone mineralization independent of BMP2.

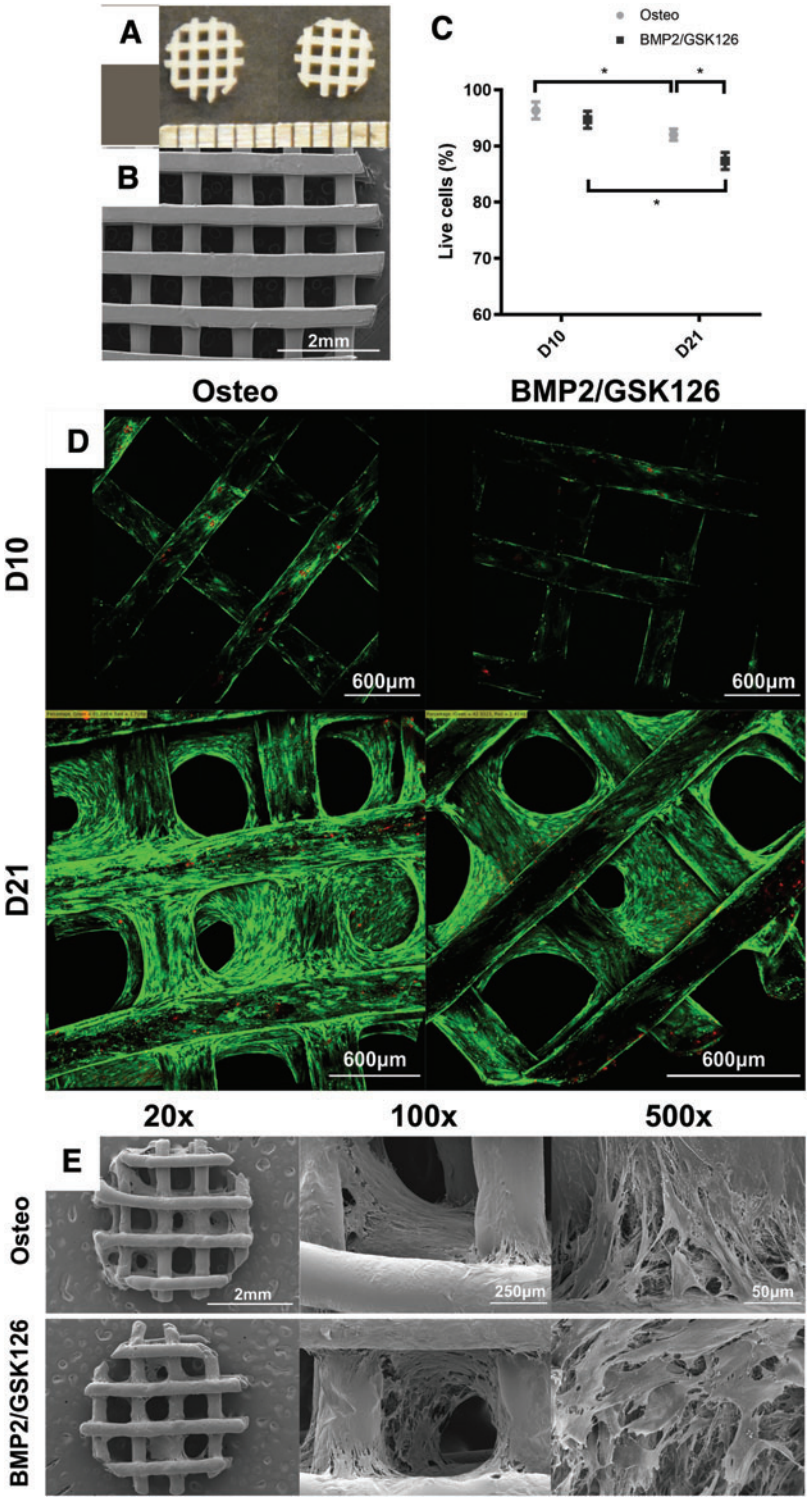

FIG. 1. Characterization of the 3-mm-diameter, 600-μm porosity mPCL scaffold, where **(A)** depicts the photograph of the scaffold and **(B)** is an SEM image of the scaffold. Cell viability analysis on seeded scaffolds with calcein acetoxymethyl (*green*, live cells) and ethidium homodimer-1 (*red*, dead cells), where **(C)** illustrates the percentage of live cells on a seeded scaffold at D10 and D21 time points ($n = 3$, mean ± standard deviation) and **(D)** presents the representative images of seeded scaffolds at D10 and D21 time points. **(E)** The SEM of the cellularized scaffold after 10 days of culture in osteogenic medium ± BMP2/GSK126 treatment with dense extracellular matrix fibers visible at 20×, 100×, and 500× magnification. * denotes statistical significance. BMP2, bone morphogenetic protein 2; mPCL, medical-grade polycaprolactone; SEM, scanning electron microscopy. Color images are available online.

In vivo *characterization*

microCT of the samples at 8 weeks postimplantation demonstrated no significant bone formation within the scaffolds. Histology showed that the scaffolds were fully infiltrated with host cells and that some remaining hydrogel could be seen across all groups along with the presence of fatty marrow in the central portion of the scaffold (Fig. 5). There was no mature bone observed in any of the treatment groups corroborating the microCT results. Sirius red S staining demonstrated that the region with dense cellularity was also composed by important collagen deposition, possibly indicating early mineralization in all samples except the Control and Osteo scaffolds (Fig. 6, indicated by "*").

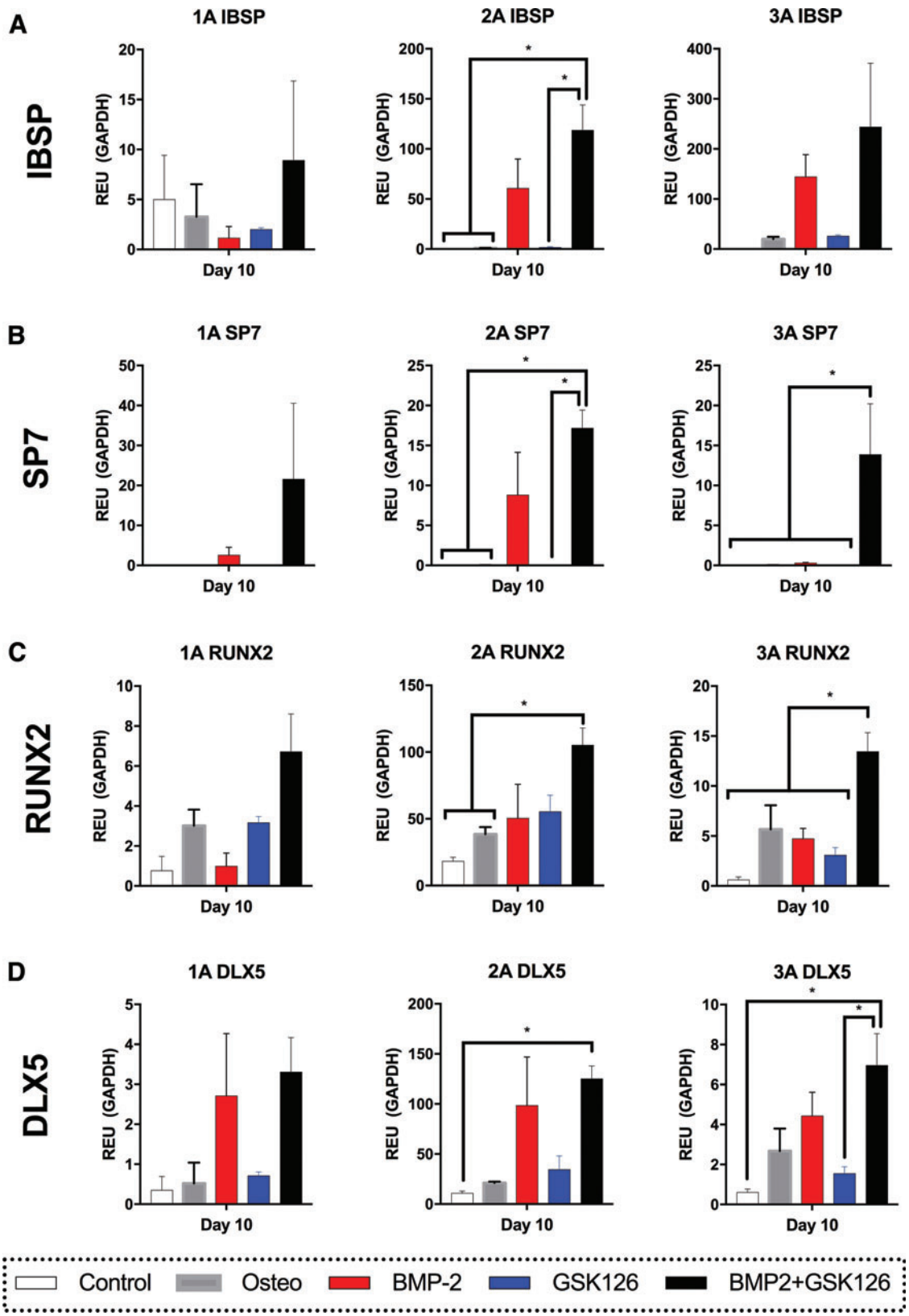

FIG. 2. RTqPCR analysis for gene expression of osteogenic genes [**(A)** *IBSP*, **(B)** *SP7*, **(C)** *RUNX2*, **(D)** *DLX5*] for the three donors after Day 10 of *in vitro* culture. ($n = 3$ per donor, mean ± standard mean error). * denotes statistical significance. RTqPCR, realtime quantitative polymerase chain reaction. Color images are available online.

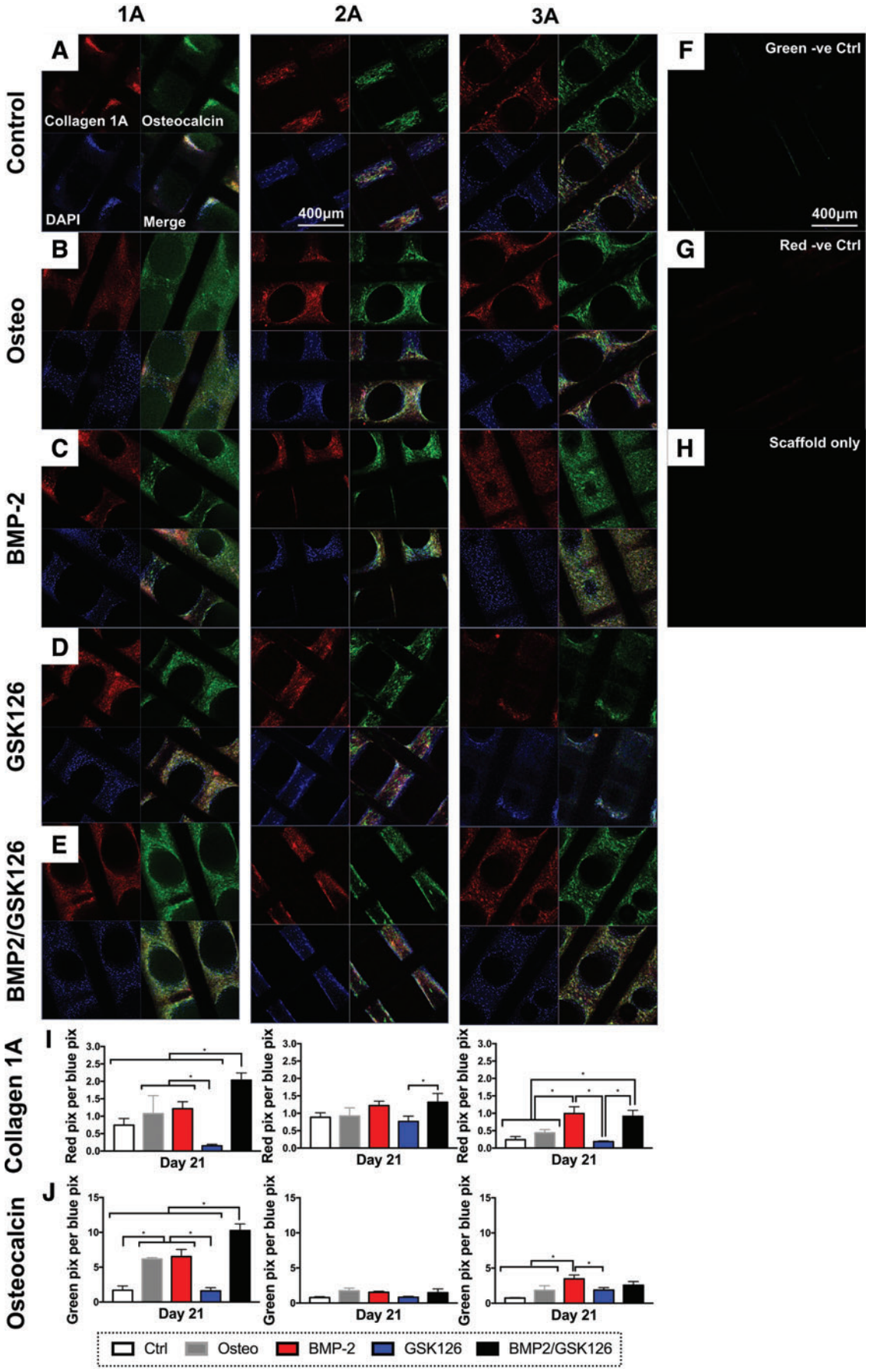

FIG. 3. IF staining of the scaffolds at 21 days postseeding showing **(A–E)** *COL1A1* (*red*) and *BGLAP* (*green*) staining. Samples were counterstained with DAPI to visualize the cell nuclei. **(F, G)** IF staining of sample without primary antibody. **(H)** IF staining of PCL scaffold without cells. **(I, J)** Semiquantification of IF staining for COL1A1 and BGLAP across the three donors normalized for number of *blue* pixels ($n=3$ per donor, mean ± standard deviation). * denotes statistical significance. IF, immunofluorescence. Color images are available online.

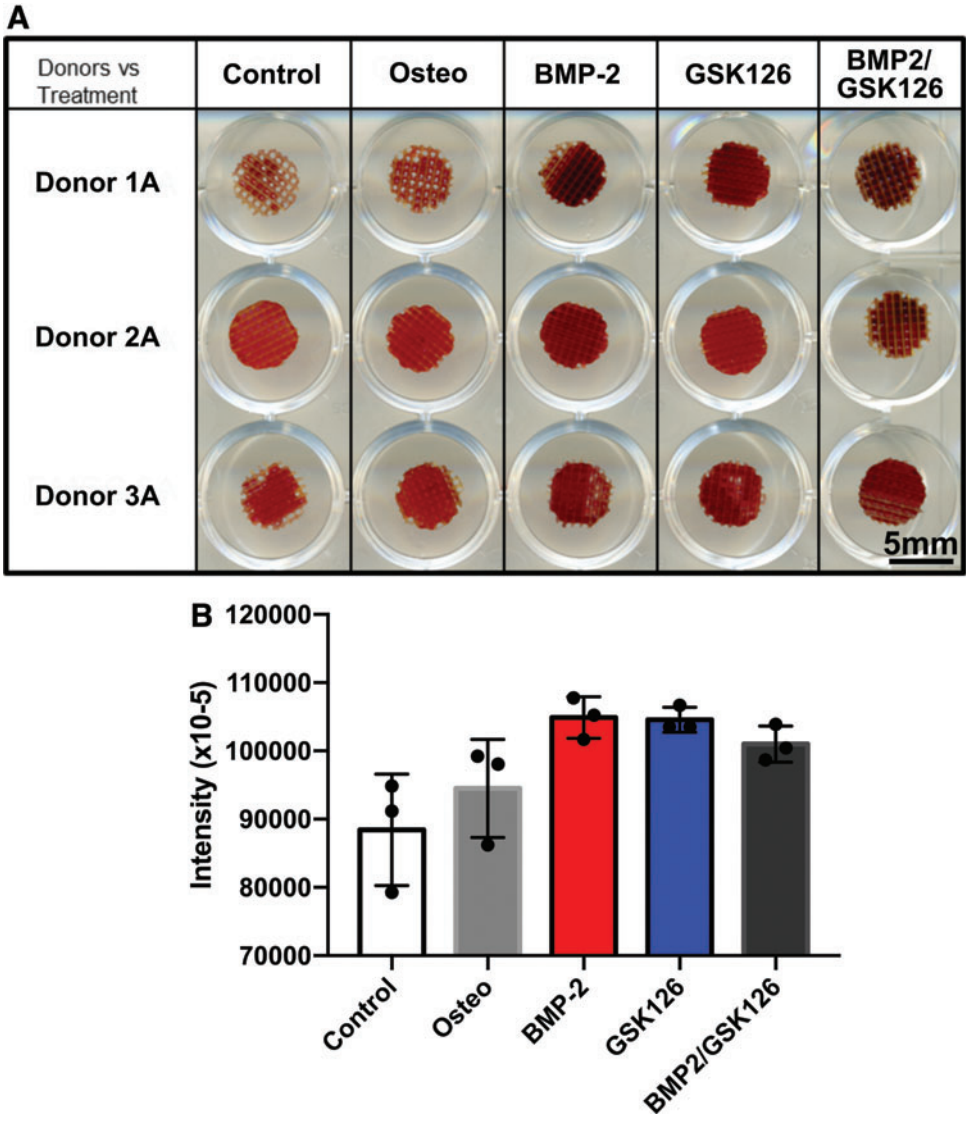

FIG. 4. Alizarin red staining of BMSCs on the scaffold. **(A)** Scan image of stained scaffolds. **(B)** Intensity of absorbance for Alizarin red staining averaged over the three donors ($n = 3$ per donor, mean ± standard deviation). BMSC, bone marrow-derived mesenchymal stem cell. Color images are available online.

The HA/gelatin hydrogel was incorporated into the scaffold to support the BMSCs and provide ECM in bone formation. The BMP2/GSK126 groups displayed less hydrogel remaining after 8 weeks compared with the other groups, although there was no statistically significant difference. This may indicate greater macrophage activity and is supported by the higher vasculature density in the BMP2/GSK126 group.

Histomorphometrical analysis revealed that the BMP2 and BMP2/GSK126 treatment groups demonstrated a significantly higher vasculature density of 43 ± 10 blood vessels per $1\,mm^2$ and 39 ± 9 blood vessels per $1\,mm^2$, respectively, when compared with the treatment groups (Control and Osteo) (Fig. 7A), and this was consistently observed for all donors. There was no significant difference between the Osteo and GSK126 treatment for inducing angiogenesis. While histomorphometry demonstrated a slight increase in the area of early mineralization for BMP2, GSK126, and BMP2/GSK126 groups, it only reached statistical significance for the BMP2 preconditioning for Donor 3A.

Discussion

This study has investigated the effects of preconditioning BMSCs seeded on 3D scaffolds with BMP2, GSK126, and a combination of these two biological cues with subsequent implantation into an ectopic mouse model. The rationale of pretreating cells with GSK126, a known inhibitor of EZH2, originates from its involvement in osteogenesis. Indeed, a landmark study[35] demonstrated that EZH2 is downregulated once mesenchymal stem cells (MSCs) have committed to the osteogenic lineage. Furthermore, inhibition of EZH2 has resulted in downregulation of cellular proliferation as well as increased synthesis of bone-related ECM, thereby supporting bone healing.[35,36] This trend was confirmed in MC3T3 preosteoblasts where EZH2 inhibition resulted in increased expression of wingless-related integrated site (Wnt10b) and parathyroid hormone 1 receptor (Pth1r) bone stimulatory proteins via the BMP-dependent phosphorylation of Smad1/5.[34] Administration of both BMP2 and GSK126 in conjunction resulted in significantly more bone formation in MC3T3 preosteoblasts.[34] Our study utilized

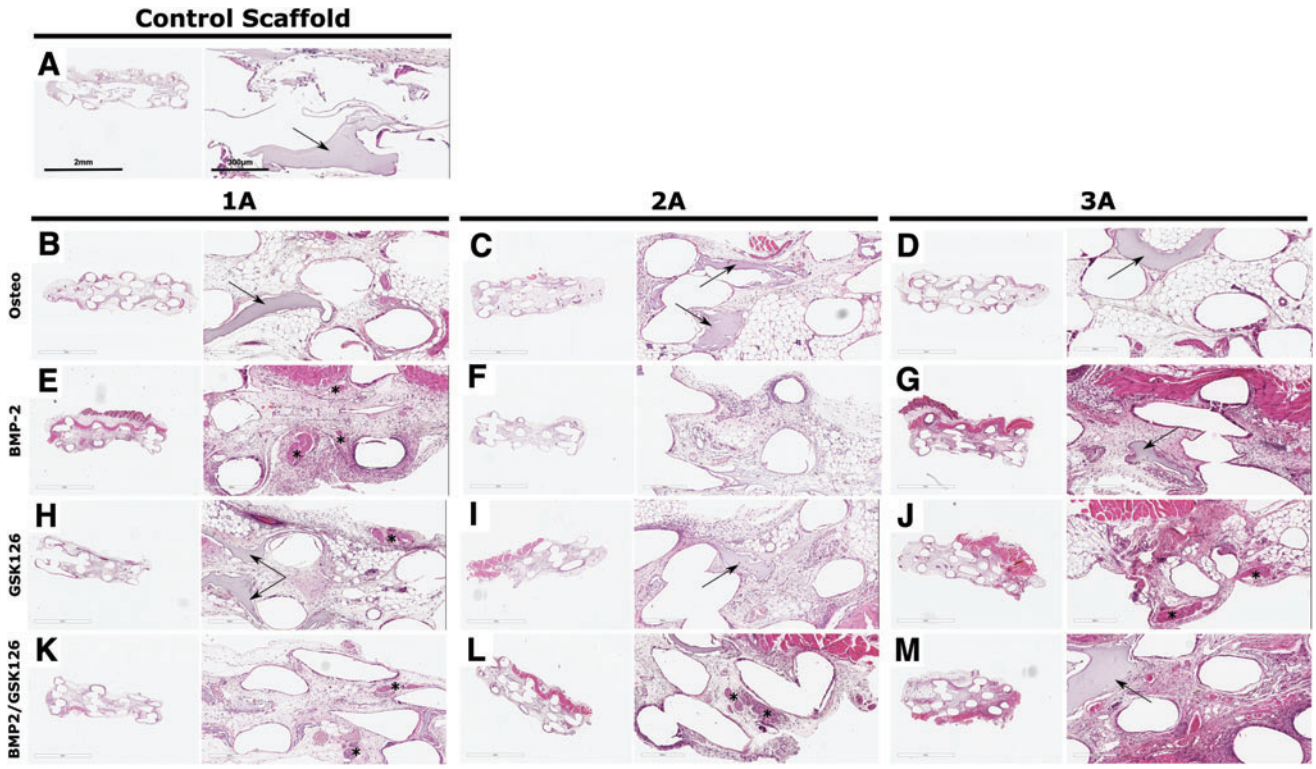

FIG. 5. H&E staining of BMSC-seeded constructs implanted for 8 weeks for the control scaffold and each of the three donors under the four treatment groups **(A–M)**. An ''*'' has been used to highlight early mineralization and the *arrows* indicate the remaining hydrogel within the scaffold. H&E, hematoxylin and eosin. Color images are available online.

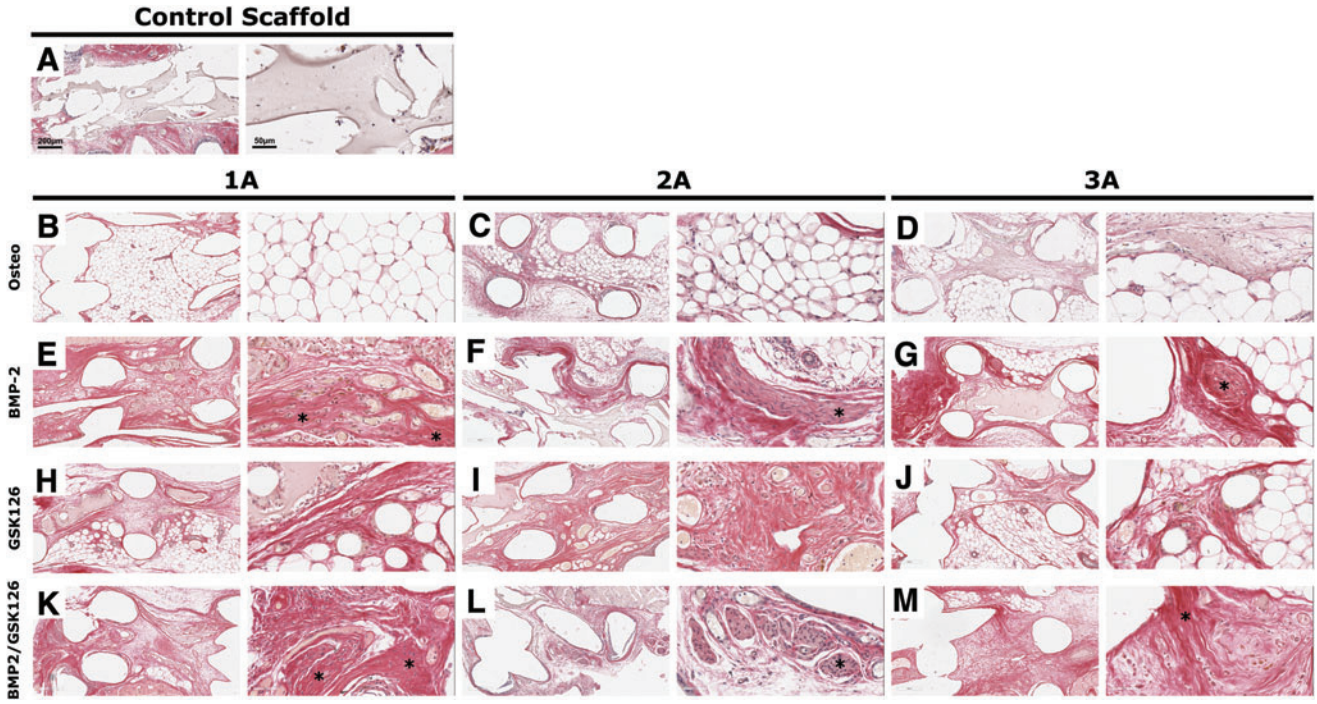

FIG. 6. Sirius red staining of BMSC-seeded constructs implanted for 8 weeks for the control scaffold and each of the three donors under the four treatment groups **(A–M)**. An ''*'' has been used to highlight early mineralization. Color images are available online.

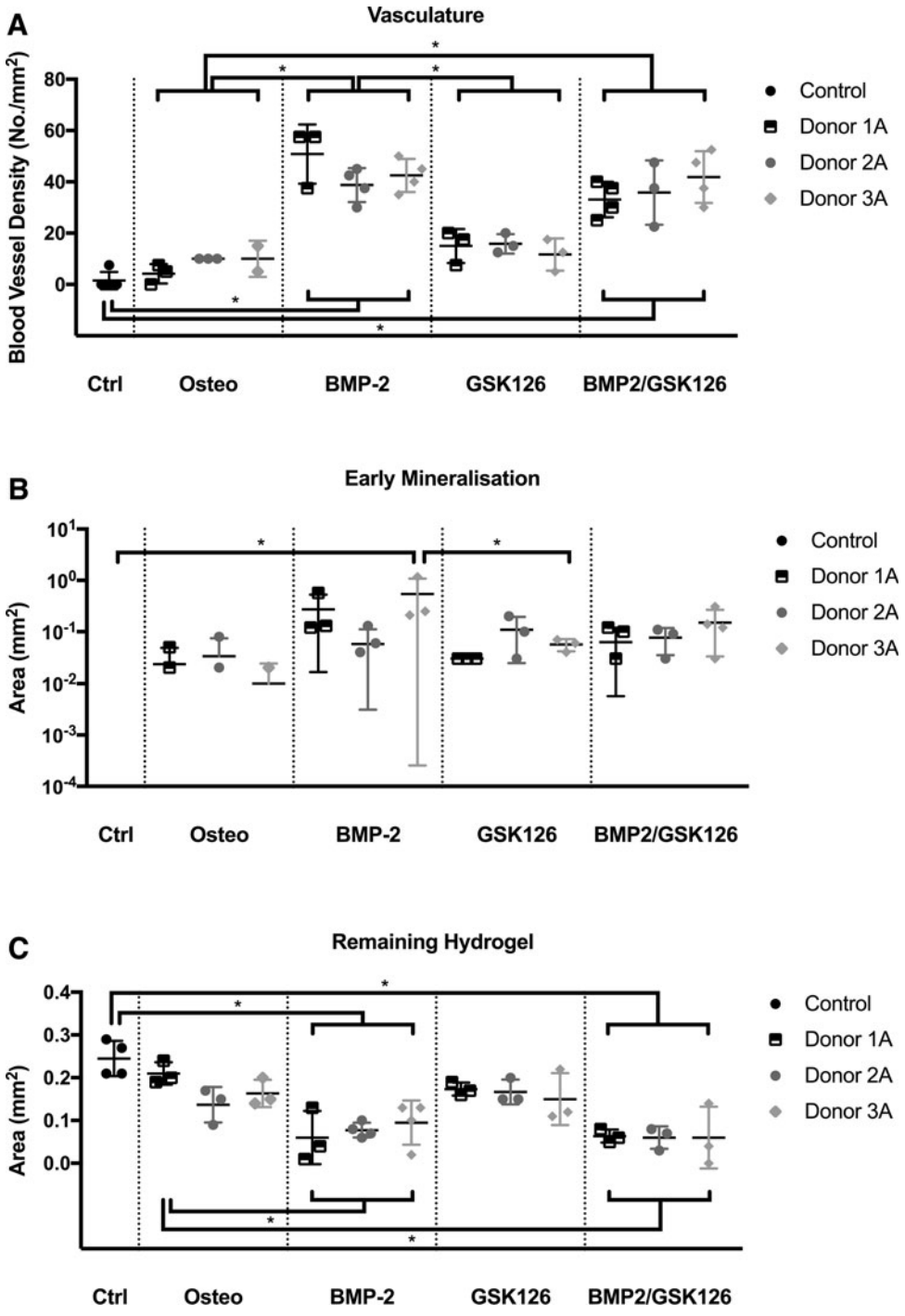

FIG. 7. Histomorphometry analysis of **(A)** vascularization, **(B)** early mineralization, and **(C)** hydrogel remaining in the samples at 8 weeks. An "*" denotes statistical differences ($p < 0.05$) ($n = 3$ per donor, mean ± standard deviation).

primary cells isolated from human bone marrow and supports previous studies by our research group[34,35,44] that GSK126 can be used to improve bone tissue engineering. In particular, the study has highlighted for the first time the potential of using GSK126 in 3D cell cultures in 3D-printed scaffolds. BMP2 was used as a positive control and it was observed that GSK126 did not abolish BMP2's osteogenic effect.

The importance of EZH2 inhibition toward osteogenic differentiation was previously demonstrated in an osteoporotic estrogen-deficient mouse model by daily injecting 50 mg/kg GSK126 over 5 weeks, which resulted in increased bone formation.[34] While systemic delivery of EZH2 inhibitors such as GSK126 may cause overt adverse effects, local application of these inhibitors for short periods of time can be considered for the treatment of bone trauma such as nonunion fractures, spinal fusion, and critical-sized defect models.[34,35,44] Because EZH2 inhibition may compromise cell proliferation in addition to enhancing osteogenic gene expression,[34,35,44] our current strategy involved the treatment of MSC with GSK126 during a determined period *in vitro* before *in vivo* implantation. Our preconditioning

strategy also involved the stimulation of the cells only for a reduced period of time to mitigate any potential DNA damage inflicted by a prolonged *in vitro* culture, which may be detrimental to differentiation capacity.[57] Interestingly, our data demonstrated that a pretreatment of 6 days resulted in long-term upregulation of bone-related ECM components, suggesting a memory effect of the differentiation cocktail.

The analysis of gene expression in the *in vitro* experimentation supported the above results of using EZH2 to promote osteogenic differentiation *in vitro* and illustrated clear trends in upregulated expression of *IBSP*, *SP7*, *Runx2*, and *DLX5* in the BMP2 and BMP2/GSK126 groups. The addition of both BMP2 and GSK126 into cell culture acted to further improve osteogenesis in the BMSCs. This was reflected in the expression of *COL1A1* and *BGLAP* proteins semiquantified via IF staining in Donors 1A and 3A. However, this strong commitment toward osteogenesis *in vitro* differentiation was not translated into *in vivo* bone formation. Indeed, none of the retrieved samples resulted in bone mineralization at 8 weeks postimplantation.

Interestingly, early signs of bone formation, as demonstrated by the presence of areas of high cell condensation within a dense collagen matrix, were consistently observed for the specimens pretreated with BMP2, and to a smaller extent with BMP2/GSK126. This indicates that the assessment of *in vitro* preconditioning onto the bone formation efficacy may have required prolonged *in vivo* implantation to lead to ectopic osteogenesis.

The site of implantation may have played a significant role in facilitating ectopic bone formation. Previous studies by our group revealed that MC3T3 osteoblasts can be preconditioned by cotreatment with BMP2 and GSK126, and that bone maturation in a murine calvarial defect is stimulated upon local administration of BMP2 and/or GSK126.[44] These studies indicate that a calvarial defect model is more fitting to assess osteogenesis and the use of a subcutaneous ectopic model explains why a lack of bone formation was observed in this study. Indeed, it has been suggested that intramuscular implantation, as opposed to subcutaneous implantation, generally increases the frequency of bone formation in osteogenic materials.[58]

Despite these limitations, a subcutaneous animal model would still demonstrate the mineralization of cells independent of native bone cells. While natural biomaterials have greater bioactivity, PCL is commonly used in tissue engineering applications due to its superior mechanical properties for bone regeneration and is unlikely to have prevented bone formation.[54,59–62] We justified the selection of a subcutaneous model as it was a convenient method for testing multiple different combinations as a screening process before proceeding to *in vivo* testing with a bony defect model. In addition, as we were focusing on accelerating bone induction rather than bone formation, a subcutaneous model was an appropriate choice. Another explanation for the potentially delayed osteogenesis comes from the number of implanted cells as several studies demonstrated that a cell number threshold is required to trigger a biological response.

There appears to be evidence of hemopoiesis upon subcutaneous implantation of treated BMSCs when preconditioned with any of the biological cues, used separately or in combination. This finding is not unusual as other MSC-related constructs have been shown to exhibit some form of vascularization as skin capillaries at implantation sites naturally infiltrate scaffold following incision. Therefore, it is not possible for us to conclude that preconditioning increases vascularization, although it remains a possibility that preconditioning may enhance this natural capillarization process that is generally observed for BMSC implants. The development of a vascularized network is of importance in the context of bone regeneration, as neovascularization is essential for enabling subsequent bone formation.[63] The preconditioning with biological cues may enhance greater bone healing in a defect by facilitating angiogenesis.

The utilization of 3D-printed constructs with pretreated cells in this study has potentially significant advantages in facilitating spatially accurate cells deliver and enhanced cell retention in the implanted site. However, our present study involving preconditioning of cells on a 3D scaffold and suggests that ectopic bone formation in a 3D environment may require different preconditioning settings (e.g., concentration and length) to achieve bone formation. Overall, the utilization of EZH2 inhibitors to modulate gene expression in favor of bone healing has been demonstrated *in vitro* in a tissue engineering strategy. Our study will pave the way to developing tissue engineering strategies involving GSK126 as an adjuvant to increase the effects of BMP2 for stimulating cells of interest on a 3D scaffold.

Conclusion

This study reported the use of the EZH2 inhibitor GSK126 to inactivate epigenetic mechanisms that suppress osteogenesis to augment BMP2-mediated bone healing. The pretreatment of BMSCs with BMP2/GSK126 upregulated gene expression for osteogenesis *in vitro* but did not translate into significant bone mineralization after 8 weeks *in vivo*. However, the increased angiogenesis observed in both the BMP2 and BMP2/GSK126 groups may suggest a greater potential for mineralization in a bone defect model. Further studies are required to determine whether the use of BMP2 with GSK126 may negate the need or reduce the normal BMP2 dosage *in vivo* for stimulating bone regeneration.

Acknowledgments

The researchers thank the support of the Mayo Clinic Department of Orthopedic Surgery and the Mayo Clinic Department of Biochemistry and Molecular Biology in undertaking this project. They also thank the Queensland University of Technology Histology Laboratory for assisting in relevant data analysis.

Disclosure Statement

No competing financial interests exist.

Funding Information

The work was supported in part by a National Institutes of Health grant number: R01 AR049069.

References

1. Azi, M.L., Aprato, A., Santi, I., Kfuri, M., Jr., Masse, A., and Joeris, A. Autologous bone graft in the treatment of post-traumatic bone defects: a systematic review and meta-analysis. BMC Musculoskelet Disord **17,** 465, 2016.

2. Tosounidis, T.H., and Giannoudis, P.V. Biological facet of segmental bone loss reconstruction. J Orthop Trauma **31 Suppl 5,** S27, 2017.
3. Hofmann, A., Gorbulev, S., Guehring, T., *et al.* Autologous iliac bone graft compared with biphasic hydroxyapatite and calcium sulfate cement for the treatment of bone defects in tibial plateau fractures: a prospective, randomized, Open-Label, Multicenter Study. J Bone Joint Surg Am **102,** 179, 2020.
4. Van der Stok, J., Hartholt, K.A., Schoenmakers, D.A.L., and Arts, J.J.C. The available evidence on demineralised bone matrix in trauma and orthopaedic surgery: a systematic review. Bone Joint Res **6,** 423, 2017.
5. Velasco, M., Narváez-Tovar, C., and Garzón-Alvarado, D. Design, materials and mechanobiology of biodegradable scaffolds for bone tissue engineering. Biomed Res Int **2015,** 1, 2015.
6. Chong, A., and Chang, J. Tissue engineering for the hand surgeon: a clinical perspective. J Hand Surg **31A,** 349, 2006.
7. Temple, J.P., Hutton, D.L., Hung, B.P., *et al.* Engineering anatomically shaped vascularized bone grafts with hASCs and 3D-printed PCL scaffolds. J Biomed Mater Res A **102,** 4317, 2014.
8. Guo, L., Min, S., Su, Y., *et al.* Collagen sponge functionalized with chimeric anti-BMP-2 monoclonal antibody mediates repair of nonunion tibia defects in a nonhuman primate model: an exploratory study. J Biomater Appl **32,** 425, 2017.
9. Durham, E.L., Howie, R.N., Hall, S., *et al.* Optimizing bone wound healing using BMP2 with absorbable collagen sponge and Talymed nanofiber scaffold. J Transl Med **16,** 321, 2018.
10. Wu, J., Zheng, A., Liu, Y., *et al.* Enhanced bone regeneration of the silk fibroin electrospun scaffolds through the modification of the graphene oxide functionalized by BMP-2 peptide. Int J Nanomed **14,** 733, 2019.
11. Ruehle, M.A., Li, M.A., Cheng, A., Krishnan, L., Willett, N.J., and Guldberg, R.E. Decorin-supplemented collagen hydrogels for the co-delivery of bone morphogenetic protein-2 and microvascular fragments to a composite bone-muscle injury model with impaired vascularization. Acta Biomater **93,** 210, 2019.
12. Krishnan, L., Priddy, L.B., Esancy, C., *et al.* Hydrogel-based delivery of rhBMP-2 improves healing of large bone defects compared with autograft. Clin Orthop Relat Res **473,** 2885, 2015.
13. Bhakta, G., Ekaputra, A.K., Rai, B., *et al.* Fabrication of polycaprolactone-silanated β-tricalcium phosphate-heparan sulfate scaffolds for spinal fusion applications. Spine J **18,** 818, 2018.
14. Berner, A., Woodruff, M.A., Lam, C.X., *et al.* Effects of scaffold architecture on cranial bone healing. Int J Oral Maxillofac Surg **43,** 506, 2014.
15. Cipitria, A., Wagermaier, W., Zaslansky, P., *et al.* BMP delivery complements the guiding effect of scaffold architecture without altering bone microstructure in critical-sized long bone defects: a multiscale analysis. Acta Biomater **23,** 282, 2015.
16. Chai, Y.C., Roberts, S.J., Desmet, E., *et al.* Mechanisms of ectopic bone formation by human osteoprogenitor cells on CaP biomaterial carriers. Biomaterials **33,** 3127, 2012.
17. Vaquette, C., Ivanovski, S., Hamlet, S.M., and Hutmacher, D.W. Effect of culture conditions and calcium phosphate coating on ectopic bone formation. Biomaterials **34,** 5538, 2013.
18. Bandyopadhyay, A., Tsuji, K., Cox, K., Harfe, B.D., Rosen, V., and Tabin, C.J. Genetic analysis of the roles of BMP2, BMP4, and BMP7 in limb patterning and skeletogenesis. PLoS Genet **2,** e216, 2006.
19. Cipitria, A., Reichert, J.C., Epari, D.R., *et al.* Polycaprolactone scaffold and reduced rhBMP-7 dose for the regeneration of critical-sized defects in sheep tibiae. Biomaterials **34,** 9960, 2013.
20. Reichert, J.C., Cipitria, A., Epari, D.R., *et al.* A tissue engineering solution for segmental defect regeneration in load-bearing long bones. Sci Transl Med **4,** 141ra93, 2012.
21. Cipitria, A., Wagermaier, W., Zaslansky, P., *et al.* BMP delivery complements the guiding effect of scaffold architecture without altering bone microstructure in critical-sized long bone defects: a multiscale analysis. Acta Biomater **23,** 282, 2015.
22. Rahman, M.S., Akhtar, N., Jamil, H.M., Banik, R.S., and Asaduzzaman, S.M. TGF-beta/BMP signaling and other molecular events: regulation of osteoblastogenesis and bone formation. Bone Res **3,** 15005, 2015.
23. Wang, R.N., Green, J., Wang, Z., *et al.* Bone morphogenetic protein (BMP) signaling in development and human diseases. Genes Dis **1,** 87, 2014.
24. Ryoo, H.M., Lee, M.H., and Kim, Y.J. Critical molecular switches involved in BMP-2-induced osteogenic differentiation of mesenchymal cells. Gene **366,** 51, 2006.
25. van Wijnen, A.J., and Westendorf, J.J. Epigenetics as a new frontier in orthopedic regenerative medicine and oncology. J Orthop Res **37,** 1465, 2019.
26. Waddington, C.H. The epigenotype. Endeavour **1,** 18, 1942.
27. Jaenisch, R., and Bird, A. Epigenetic regulation of gene expression: how the genome integrates intrinsic and environmental signals. Nat Genet **33 Suppl,** 245, 2003.
28. Zaidi, S.K., Young, D.W., Montecino, M.A., *et al.* Mitotic bookmarking of genes: a novel dimension to epigenetic control. Nat Rev Genet **11,** 583, 2010.
29. van Wijnen, A.J., van de Peppel, J., van Leeuwen, J.P., *et al.* MicroRNA functions in osteogenesis and dysfunctions in osteoporosis. Curr Osteoporos Rep **11,** 72, 2013.
30. Lian, J.B., Stein, G.S., van Wijnen, A.J., *et al.* MicroRNA control of bone formation and homeostasis. Nat Rev Endocrinol **8,** 212, 2012.
31. Varela, N., Aranguiz, A., Lizama, C., *et al.* Mitotic inheritance of mRNA facilitates translational activation of the osteogenic-lineage commitment factor Runx2 in progeny of osteoblastic cells. J Cell Physiol **231,** 1001, 2016.
32. Gordon, J.A., Stein, J.L., Westendorf, J.J., and van Wijnen, A.J. Chromatin modifiers and histone modifications in bone formation, regeneration, and therapeutic intervention for bone-related disease. Bone **81,** 739, 2015.
33. Cho, Y.D., Yoon, W.J., Kim, W.J., *et al.* Epigenetic modifications and canonical wingless/int-1 class (WNT) signaling enable trans-differentiation of nonosteogenic cells into osteoblasts. J Biol Chem **289,** 20120, 2014.
34. Dudakovic, A., Camilleri, E.T., Riester, S.M., *et al.* Enhancer of zeste homolog 2 inhibition stimulates bone formation and mitigates bone loss caused by ovariectomy in skeletally mature mice. J Biol Chem **291,** 24594, 2016.
35. Dudakovic, A., Camilleri, E.T., Xu, F., *et al.* Epigenetic control of skeletal development by the histone methyltransferase Ezh2. J Biol Chem **290,** 27604, 2015.

36. Hemming, S., Cakouros, D., Isenmann, S., *et al.* EZH2 and KDM6A act as an epigenetic switch to regulate mesenchymal stem cell lineage specification. Stem Cells **32,** 802, 2014.
37. Cho, Y.D., Kim, W.J., Yoon, W.J., *et al.* Wnt3a stimulates Mepe, matrix extracellular phosphoglycoprotein, expression directly by the activation of the canonical Wnt signaling pathway and indirectly through the stimulation of autocrine Bmp-2 expression. J Cell Physiol **227,** 2287, 2012.
38. Margueron, R., and Reinberg, D. The Polycomb complex PRC2 and its mark in life. Nature **469,** 343, 2011.
39. Wei, Y., Chen, Y.H., Li, L.Y., *et al.* CDK1-dependent phosphorylation of EZH2 suppresses methylation of H3K27 and promotes osteogenic differentiation of human mesenchymal stem cells. Nat Cell Biol **13,** 87, 2011.
40. Wang, H., Meng, Y., Cui, Q., *et al.* MiR-101 Targets the EZH2/Wnt/β-catenin the pathway to promote the osteogenic differentiation of human bone marrow-derived mesenchymal stem cells. Sci Rep **6,** 36988, 2016.
41. Zhu, X.X., Yan, Y.W., Chen, D., *et al.* Long non-coding RNA HoxA-AS3 interacts with EZH2 to regulate lineage commitment of mesenchymal stem cells. Oncotarget **7,** 63561, 2016.
42. Chen, Y.H., Chung, C.C., Liu, Y.C., *et al.* Enhancer of zeste homolog 2 and histone deacetylase 9c regulate age-dependent mesenchymal stem cell differentiation into osteoblasts and adipocytes. Stem Cells **34,** 2183, 2016.
43. Jing, H., Liao, L., An, Y., *et al.* Suppression of EZH2 prevents the shift of osteoporotic MSC fate to adipocyte and enhances bone formation during osteoporosis. Mol Ther **24,** 217, 2016.
44. Dudakovic, A., Samsonraj, R.M., Paradise, C.R., *et al.* Inhibition of the epigenetic suppressor EZH2 primes osteogenic differentiation mediated by BMP2. J Biol Chem **295,** 7877, 2020.
45. Dudakovic, A., and Wijnen, A. Epigenetic control of osteoblast differentiation by enhancer of zeste homolog 2 (EZH2). Curr Mol Biol Rep **3,** 1, 2017.
46. Chen, Y.H., Yeh, F.L., Yeh, S.P., *et al.* Myocyte enhancer factor-2 interacting transcriptional repressor (MITR) is a switch that promotes osteogenesis and inhibits adipogenesis of mesenchymal stem cells by inactivating peroxisome proliferator-activated receptor gamma-2. J Biol Chem **286,** 10671, 2011.
47. Morin, R.D., Johnson, N.A., Severson, T.M., *et al.* Somatic mutations altering EZH2 (Tyr641) in follicular and diffuse large B-cell lymphomas of germinal-center origin. Nat Genet **42,** 181, 2010.
48. Kleer, C.G., Cao, Q., Varambally, S., *et al.* EZH2 is a marker of aggressive breast cancer and promotes neoplastic transformation of breast epithelial cells. Proc Natl Acad Sci U S A **100,** 11606, 2003.
49. Varambally, S., Dhanasekaran, S.M., Zhou, M., *et al.* The polycomb group protein EZH2 is involved in progression of prostate cancer. Nature **419,** 624, 2002.
50. Comet, I., Riising, E.M., Leblanc, B., and Helin, K. Maintaining cell identity: PRC2-mediated regulation of transcription and cancer. Nat Rev Cancer **16,** 803, 2016.
51. McCabe, M.T., Ott, H.M., Ganji, G., *et al.* EZH2 inhibition as a therapeutic strategy for lymphoma with EZH2-activating mutations. Nature **492,** 108, 2012.
52. Lui, H., Bindra, R., Baldwin, J., Ivanovski, S., and Vaquette, C. Additively manufactured multiphasic bone–ligament–bone scaffold for scapholunate interosseous ligament reconstruction. Adv Healthc Mater **8,** 1900133, 2019.
53. Samsonraj, R.M., Rai, B., Sathiyanathan, P., *et al.* Establishing criteria for human mesenchymal stem cell potency. Stem Cells **33,** 1878, 2015.
54. Lui, H., Bindra, R., Baldwin, J., Ivanovski, S., and Vaquette, C. Additively manufactured multiphasic bone–ligament–bone scaffold for scapholunate interosseous ligament reconstruction. Adv Health Care Mater **0,** 1900133, 2019.
55. Berner, A., Reichert, J.C., Woodruff, M.A., *et al.* Autologous vs. allogenic mesenchymal progenitor cells for the reconstruction of critical sized segmental tibial bone defects in aged sheep. Acta Biomater **9,** 7874, 2013.
56. Sudheesh Kumar, P.T., Hashimi, S., Saifzadeh, S., Ivanovski, S., and Vaquette, C. Additively manufactured biphasic construct loaded with BMP-2 for vertical bone regeneration: a pilot study in rabbit. Mater Sci Eng C Mater Biol Appl **92,** 554, 2018.
57. Alves, H., Munoz-Najar, U., De Wit, J., *et al.* A link between the accumulation of DNA damage and loss of multipotency of human mesenchymal stromal cells. J Cell Mol Med **14,** 2729, 2010.
58. Barradas, A.M., Yuan, H., van Blitterswijk, C.A., and Habibovic, P. Osteoinductive biomaterials: current knowledge of properties, experimental models and biological mechanisms. Eur Cells Mater **21,** 407, 2011.
59. Lui, H., Vaquette, C., Denbeigh, J.M., Bindra, R., Kakar, S., and van Wijnen, A.J. Multiphasic scaffold for scapholunate interosseous ligament reconstruction: a study in the rabbit knee. J Orthop Res 2020 [Epub ahead of print]; DOI: 10.1002/jor.24785.
60. McGovern, J.A., Griffin, M., and Hutmacher, D.W. Animal models for bone tissue engineering and modelling disease. Dis Model Mech **11,** dmm033084, 2018.
61. Poh, P.S.P., Hutmacher, D.W., Holzapfel, B.M., Solanki, A.K., Stevens, M.M., and Woodruff, M.A. In vitro and in vivo bone formation potential of surface calcium phosphate-coated polycaprolactone and polycaprolactone/bioactive glass composite scaffolds. Acta Biomater **30,** 319, 2016.
62. Hamlet, S.M., Vaquette, C., Shah, A., Hutmacher, D.W., and Ivanovski, S. 3-Dimensional functionalized polycaprolactone-hyaluronic acid hydrogel constructs for bone tissue engineering. J Clin Periodontol **44,** 428, 2017.
63. Novosel, E.C., Kleinhans, C., and Kluger, P.J. Vascularization is the key challenge in tissue engineering. Adv Drug Deliv Rev **63,** 300, 2011.

Address correspondence to:
Andre J. van Wijnen, PhD
Departments of Orthopedic Surgery
and Biochemistry and Molecular Biology
Mayo Clinic
200 1st Street SW
Rochester, MN 55905
USA

E-mail: vanwijnen.andre@mayo.edu

Received: July 28, 2020
Accepted: October 29, 2020
Online Publication Date: January 12, 2021

(*Appendix follows* →)

Appendix

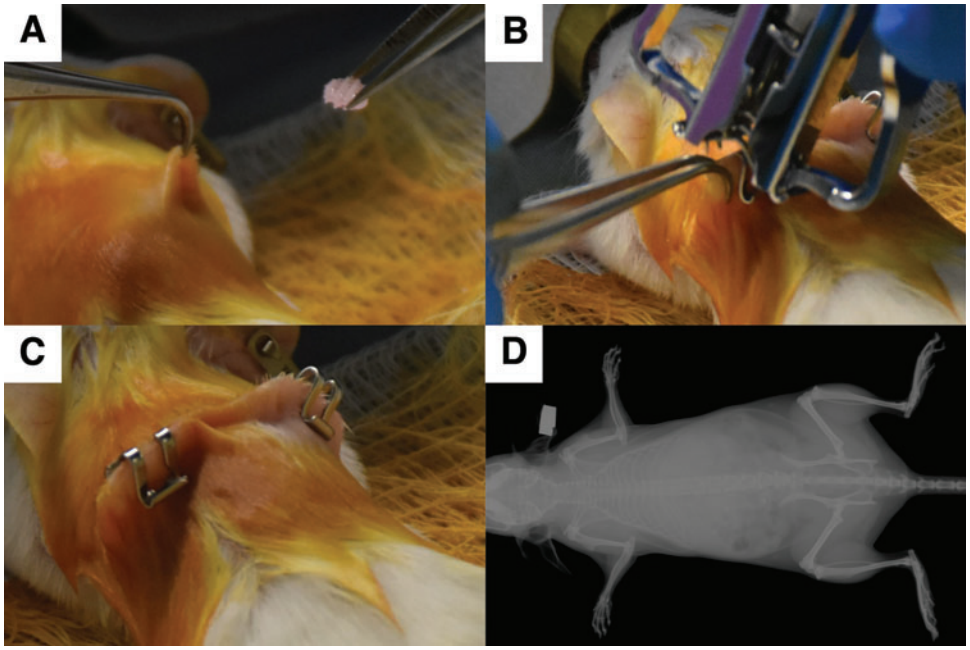

APPENDIX FIG. A1. Ectopic implantation procedure into female SCID mice. **(A)** Placement of the seeded scaffold into a subcutaneous pocket. **(B, C)** Closure of wound using wound clips. **(D)** X-ray of SCID mice in the BMP2/GSK126 group before harvesting the scaffolds. No bone formation in the subcutaneous pocket was detected. This result was consistent in all treatment groups. SCID, severe combined immune deficiency. Color images are available online.